Mode Optimization for High-Resolution Electromagnetic Vortex Radar Sparse Imaging

Yitong Wang Yixin Wei Gaofeng Shu Ning Li
School of Computer and Information Engineering
Henan University
Kaifeng, China
wangyitong@henu.edu.cn, weiyixin@henu.edu.cn, gaofeng.shu@henu.edu.cn, hedalining@henu.edu.cn

2026 China Aerospace Information Technology Conference (CAIT) | 979-8-3195-1038-9/26/$31.00 ©2026 IEEE | DOI: 10.1109/CAIT70489.2026.11553578

***Abstract*—The phase characteristics of vortex electromagnetic waves offer significant potential for forward-looking radar imaging. In recent years, compressed sensing (CS) enhances orbital angular momentum (OAM) forward-looking radar imaging under limited measurements. However, its performance is often bottlenecked by the observation matrix's high mutual coherence, caused by the spatial overlap of different mode beams. To address this, we propose an OAM mode selection strategy that minimizes matrix correlation. This approach effectively alleviates the matrix's ill-conditioned nature. Simulations demonstrate that our method significantly improves imaging accuracy and stability. Notably, despite reducing the required modes by up to 33%, it narrows the impulse response width by 0.5° compared to traditional methods.**

Keywords—Orbital angular momentum (OAM), compressed sensing(CS), observation matrix, mode Optimization

I. Introduction

The orbital angular momentum (OAM) beam has attracted widespread attention in the field of radar target detection and imaging due to its unique helical phase structure and angular modulation capability [1]. Imaging systems based on vortex electromagnetic waves have been applied to various aspects such as target position estimation [2], two-dimensional imaging [3]-[5], and three-dimensional imaging [6][7].

High-resolution electromagnetic vortex imaging typically requires a large number of OAM modes. To alleviate this requirement, existing research has introduced compressed sensing (CS) theory to achieve super-resolution imaging. [8][9]. Liu et al [10] introduced sparse Bayesian learning into electromagnetic vortex imaging and achieved target reconstruction under undersampling conditions. Qu et al [11] further proposed a two-dimensional sparse-driven high-resolution electromagnetic vortex imaging method, which effectively improved the imaging performance.

Despite the significant advantages of CS in reducing the number of modes, but its imaging resolution still largely depends on the number of modes and the large-scale observation matrix constructed from finely discretized imaging scenes [12][13].

To solve this issues, existing studies have proposed improved methods from the perspectives of observation matrix structure and physical modeling. For example, Jiang et al [14] proposed a fast super-resolution imaging method by performing structured decomposition of the observation matrix based on the physical properties of vortex waves. Qu et al [15] proposed a joint representation method combining low-rank and sparse constraints, which to suppressed the influence of Bessel functions on imaging performance.

However, most of the above methods focus on improving the CS imaging algorithm itself, while paying insufficient attention to the ill-conditioned problem of the observation matrix. Zhu et al [16] optimized the observation matrix by introducing prior information, first, they used Fourier transform to obtain the coarse distribution information of the target, and then combined the correlation of the reference matrix to adjust the observation matrix. This method improves the performance of the observation matrix to a certain extent, but this method is essentially a posterior correction strategy based on prior information. Its effect is highly dependent on the accuracy of the prior information.

This paper differs from the traditional continuous OAM mode selection method by reconstructing the observation matrix from the perspective of electromagnetic measurement mechanisms. The OAM mode selection problem is transformed into an observation matrix optimization problem, and the effectiveness of the proposed method is verified through simulation.

II. Vortex Radar Imaging Model

Uniform circular arrays (UCA) can achieve the emission of multiple OAM modes by applying different phase excitations to each array element. As shown in Fig. 1, the UCA is located in the Cartesian coordinate system and consists of N array elements with an array radius of a. The azimuth angle of the nth element is represented as $\varphi_n = 2\pi(n-1)/N, n = 0,1,\dots,N-1$.

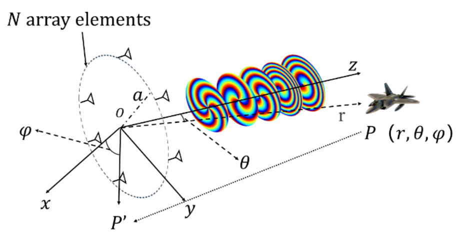

Fig. 1. Geometric model of vortex EM waves

For the target $P(r,\theta,\varphi)$, where r, θ and φ denotes the range, elevation angle, and azimuth angle, when the UCA transmits a linear frequency modulated signal, the received echo of OAM beams with the $l\text{-}th$ mode can be expressed as[5]

$$s_r(t,l) = \sum_{m=1}^{M} A_0 \frac{e^{-\mathrm{j}2kr}}{r^2}\,\mathrm{rect}\left(\frac{t-\frac{2r}{c}}{T_p}\right)\exp\left[j\pi K\left(t-\frac{2r}{c}\right)^2\right] N \mathrm{j}^{l_m} e^{\mathrm{j}l_m\varphi} J_{l_m}(ka\sin\theta) \tag{1}$$

where A_0 is a constant, T_p is the pulse duration of the transmitted signal, $\mathrm{rect}(\cdot)$ denotes the unit rectangular

This work was supported by the Plan of Science and Technology of Henan Province under Grant 262102211020.

function that defines the time interval of the echo, centered at the roundtrip delay $\tau = 2r/c$ with a duration of T_p, and K is the frequency modulation rate.

The range is obtained through pulse compression and excluded from further analysis, with the focus placed solely on the azimuth information. Therefore, after range focusing is completed and the vortex radar imaging elevation angle is θ_0, the echo signal can be expressed as

$$S_r(l) = \sum_{m=1}^{M} e^{jl_m\varphi} J_{l_m}(kasin\theta_0) \tag{2}$$

Suppose a specific set of M OAM modes, denoted by $(l_1, l_2, \dots, l_m)$, is selected for transmission. By discretizing the azimuth domain into P spatial grids, (2) can be equivalently expressed as[10]

$$S_r = S \cdot \sigma + \mathrm{n} \tag{3}$$

where S_r is the echo signal vector, S is the observation matrix, σ is the unknown scattering coefficient vector, and n denotes the unknown noise vector. The observation matrix S in (3) describes the spatial observation mechanism of the system, S can be written as

$$S = \begin{bmatrix} s_1(l_1,\varphi_1) & s_2(l_1,\varphi_2) & \cdots & s_P(l_1,\varphi_P) \\ s_1(l_2,\varphi_1) & s_2(l_2,\varphi_2) & \cdots & s_P(l_2,\varphi_P) \\ \vdots & \vdots & \ddots & \vdots \\ s_1(l_M,\varphi_1) & s_2(l_M,\varphi_2) & \cdots & s_P(l_M,\varphi_P) \end{bmatrix} \tag{4}$$

where, the $m\text{-}th$ row of the matrix reflects the phase and amplitude response of a single OAM mode over the entire discretized azimuth domain. Meanwhile, the $p\text{-}th$ column constitutes the steering vector at the p azimuth position, encompassing the comprehensive multi-mode echo characteristics for that specific spatial grid.

III. OAM Mode selection strategy and correlation analysis of observation matrix

A. Correlation Analysis

Based on the linear measurement model in (3), the successful and stable recovery of the sparse scattering vector x heavily relies on the properties of the observation matrix S. To evaluate the reconstruction performance of the selected OAM modes, we introduce the concept of mutual coherence.

Let s_p denote the $p\text{-}th$ column vector of the observation matrix S, which represents the multi-mode steering vector at the $p\text{-}th$ azimuth grid. The mutual coherence of the matrix S, denoted by $\mu(S)$, is defined as the maximum absolute and normalized inner product between any two distinct columns

$$\mu(S) = \max_{1\le z\ne b\le P} \frac{|s_z^H s_b|}{\|s_z\|_2 \|s_b\|_2} \tag{5}$$

where $(\cdot)^H$ represents the conjugate transpose operation, and $\|\cdot\|_2$ denotes the l_2-norm of a vector.

According to (2) and (5), for any two columns with azimuth angles φ_z and φ_b, we can get

$$s_z^H s_b = \sum_{m=1}^{M} J_{l_m}^2(kasin\theta) e^{jl_m(\varphi_b-\varphi_z)} \tag{6}$$

$$\|s_z\|_2^2 = \|s_b\|_2^2 = \sum_{m=1}^{M} J_{l_m}^2(kasin\theta) \tag{7}$$

To ensure that the two column vectors are orthogonal, i.e. inner product is zero, a constraint must be imposed on the phase term. According to Euler's formula, the sum of the real and imaginary parts of the complex exponent term in the complex plane must both be zero, let $\Delta\varphi = \varphi_b - \varphi_z$, $w_m = J_{l_m}^2(kasin\theta)$, thus yielding the following set of constraint equations

$$\begin{aligned} \sum_{m=1}^{M} w_m cos(l_m\Delta\varphi) = 0 \\ \sum_{m=1}^{M} w_m sin(l_m\Delta\varphi) = 0 \end{aligned} \tag{8}$$

When the selected mode sequence is symmetric about the zero ($l \in (-L, \dots L)$). Based on the parity of trigonometric functions $\sin(-x) = -\sin(x)$ and the order symmetry of the first kind of Bessel function $J_{-l}^2(x) = J_l^2(x)$, the imaginary part automatically cancels out. Therefore, the mutual coherence by observation matrix is entirely determined by the real part

$$R(\Delta\varphi) = \sum_{m=1}^{M} w_m cos(l_m\Delta\varphi) \tag{9}$$

Since cos(x) is an even function, the real terms of the corresponding terms of the positive and negative modes are superimposed in the same direction rather than canceling each other out.

Under the condition of small angular intervals $\Delta\varphi \to 0$, a second-order Taylor expansion of equation (8) is performed

$$cos(l_m\Delta\varphi) \approx 1 - (l_m\Delta\varphi)^2/2 \tag{10}$$

Substituting into equation (8), we get

$$R(\Delta\varphi) \approx \sum_{m=1}^{M} w_m - \frac{\Delta\varphi^2}{2}\sum_{m=1}^{M} w_m\, l_m^2 \tag{11}$$

Therefore, based on the above analysis, the mutual coherence can be approximated as

$$\mu(S) \approx \frac{R(\Delta\varphi)}{\sum_{m=1}^{M} w_m} = 1 - \frac{\Delta\varphi^2}{2}\frac{\sum_{m=1}^{M} w_m\, l_m^2}{\sum_{m=1}^{M} w_m} \tag{12}$$

Taking the limit $\Delta\varphi \to 0$, we obtain

$$\lim_{\Delta\varphi\to 0} \mu(S) = 1 \tag{13}$$

The above results show that as the angular grid becomes increasingly refined ($\Delta\varphi \to 0$), the mutual coherence of the observation matrix inevitably approaches unity. Under the conventional continuous-order OAM dictionary, this leads to a highly coherent sensing matrix, which violates the Restricted Isometry Property (RIP) condition required for CS and degrades reconstruction performance. Therefore, this issue cannot be addressed solely by improving reconstruction algorithms and must instead be tackled at the level of observation matrix design.

B. MODE SEQUENCE SELECTION STRATEGY

As can be seen from the above analysis, it is necessary to make reasonable selections of the modes involved in imaging in order to improve the structural characteristics of the observation matrix.

Based on the above considerations, the mode selection in this paper follows the following basic principles.

1) Low correlation principle: Modes with significant differences in spatial response are preferred to reduce the similarity between steering vectors, thereby decreasing the cross-coherence of the observation matrices, $\mu(S)$.

2) Information complementarity principle: The selected modes should cover different spatial phase change characteristics, enabling the observation matrix to characterize target information from multiple aspect thereby improving the ability to distinguish multiple targets.

3) Quantity restriction principle: To minimize the number of selected modes while ensuring imaging performance, the system's implementation complexity and computational burden should be reduced.

Based on the above analysis, the optimal design of the mode sequence can be formulated as the following constrained optimization problem

$$\min_{S_{se}} \mu\left(S(S_{se})\right) + \lambda \left|S_{se}\right| \tag{14}$$

where, S_{se} denotes the selected subset of modes, $S(S_{se})$ represents the observation matrix constructed from the selected modes, and $|S_{se}|$ is the cardinality of the selected mode set. The parameter $\lambda > 0$ is a regularization coefficient that controls the trade-off between minimizing the mutual coherence and reducing the number of selected modes. A larger λ encourages sparser mode selection with fewer modes, while a smaller λ prioritizes coherence reduction.

However, due to the complex relationship between specific modes and matrix correlation, this paper primarily focuses on introducing this conceptual framework. For practical validation, we constrain the total number of selected modes and employ an exhaustive search method to identify the optimal mode combination with the minimum correlation.

IV. SIMULATION AND RESULTS

This section designs and conducts simulation experiments to verify the effectiveness of the proposed method. A simulation scenario was constructed containing four point targets, located at positions (8.5m,10°), (8.5m,25°), (9m,10°), and (9m,25°). The relevant parameters are shown in Table I.

TABLE I. SIMULATION PARAMETERS

Parameters	Value	Unit
Carry Frequency f_c	36	GHz
Bandwidth B_w	6	GHz
Mode Range l	-10:10	
Array radius a	2	λ

To evaluate the OAM mode selection principles proposed in Section III, a representative discontinuous mode subset [−8, −6, −9, 3, −5, 8, 9, 7, 0, 10, −2, 4, −10, −1, 6] is compared with a conventional continuous mode set [−10,10] using least squares (LS) imaging. As shown in Fig. 3, simulations conducted under varying signal-to-noise ratios (SNR) demonstrate that the proposed strategy effectively resolves targets. The reconstructed imaging exhibits sharp main lobes and suppressed side lobes, maintaining excellent robustness even in high-noise environments. These results strongly verify that the discontinuous mode selection fundamentally optimizes the observation matrix structure by reducing global mutual coherence, thereby significantly enhancing the system's super-resolution imaging accuracy and noise resistance.

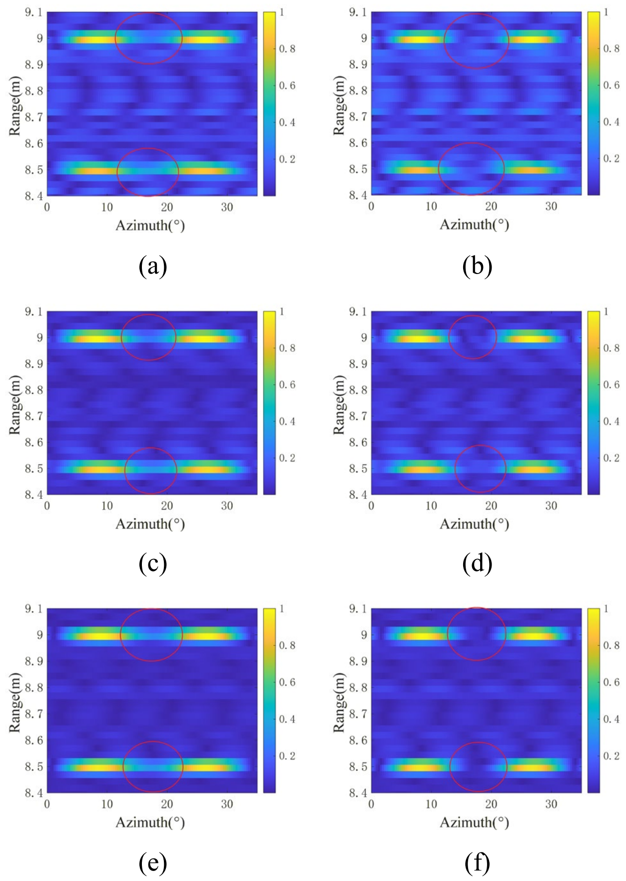

Fig. 2. Simulation results under different SNR conditions. (a) and (b) correspond to SNR = −5 dB, (c) and (d) correspond to SNR = 0 dB, and (e) and (f) correspond to SNR = 5 dB. Subfigures (a), (c), and (e) present the results obtained using the conventional mode selection method, while (b), (d), and (f) show the results of the proposed method.

To further verify the resolution advantage of the proposed mode selection strategy under different system degrees of freedom, the traditional continuous mode sequence and the proposed method under different mode ranges are compared using the LS method. Specifically, when the set mode ranges are [-7,7], [-10,10], and [-14,14], the traditional method utilizes the full continuous modes within these respective ranges. In contrast, the random mode combinations selected using the strategy proposed in this paper are [4,5,-5,0,-4,-6,-2,3,-7,6] for the [-7,7] range; [-8,-6,-9,3,-5,8,9,7,0,10,-2,4,-10,-1,6] for the [-10,10] range; and [-9,-6,-4,4,11,12,-8,-7,-13,14,2,10,-2,-14,1,-7,13,-12,5,-11] for the extended [-14,14] range.

Fig. 4 and Table II present the quantitative results of the azimuth target slices and impulse response width (IRW). The core advantage of the proposed strategy lies in achieving a narrower IRW while significantly reducing the number of required modes. Specifically, when the mode range is [-7,7], compared to the traditional method IRW of 10.65°, the proposed strategy reduces the number of modes by 33% and decreases the IRW to 9.88°. When the mode range is [-10,10], compared to the traditional method IRW of 7.60°, the proposed strategy reduces the number of modes by 28% and decreases the IRW to 6.88°. When the mode range is [-14,14], compared to the traditional method IRW of 5.50°, the proposed strategy reduces the number of modes by 31% and decreases the IRW to 4.96°.

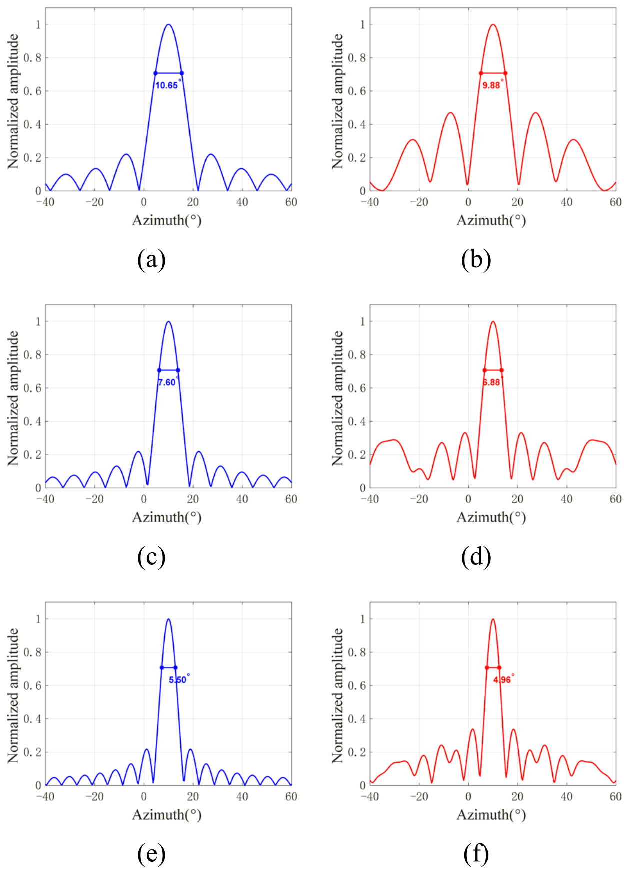

Fig. 3. Comparison of the impulse response width width between the traditional mode sequence and the proposed method under different mode ranges. (a), (c), and (e) present the results of the traditional method. (b), (d), and (f) present the results of the proposed method.

TABLE II. IMPULSE RESPONSE WIDTH OF DIFFERENT METHODS

OAM mode	Traditional method	Proposed method
[-7,7]	10.65°	9.88°
[-10,10]	7.60°	6.88°
[-14,14]	5.50°	4.96°

In summary, the proposed method reduce the redundancy limitations of traditional continuous modes, significantly reducing the system mode requirements while effectively improving the system's imaging efficiency.

V. CONCLUSION

To address the problem of excessively high correlation in the observation matrix during CS imaging with vortex radar, this paper proposes a discontinuous optimization selection strategy based on mode distribution characteristics. Simulation results show that this method effectively reduces matrix column correlation and suppresses spatial sidelobes while decreasing the number of modes used, providing a new approach to solving the ill-conditioned problem of the observation matrix.

REFERENCES

[1] S. M Barnett and L. Allen, "Orbital angular momentum and nonparaxial light beams, " Optics communications, vol. 110, no. 5-6, pp. 670-678, 1994

[2] Z. Tan, K. Liu, H. Liu, Y. Yang, F. Kuang and Y. Wang, "Object Location Estimation Method With Radar Transmitting Vortex Electromagnetic Wave," in IEEE Transactions on Antennas and Propagation, vol. 73, no. 12, pp. 10748-10756, 2025

[3] Y. Wei, G. Shu and N. Li, "Improving Orbital Angular Momentum Mode Utilization With Mode Switching Periodically in Radar Forward-Looking Imaging," in IEEE Signal Processing Letters, vol. 32, pp. 3102-3106, 2025

[4] Y. Wang, K. Liu, H. Liu and H. Wang, "High-speed Moving Target Detection Method with OAM Radar," 2024 IEEE MTT-S International Microwave Workshop Series on Advanced Materials and Processes for RF and THz Applications (IMWS-AMP), Nanjing, China, 2024, pp. 1-3

[5] K. Liu, Y. Cheng, Z. Yang, H. Wang, Y. Qin and X. Li, "Orbital-Angular-Momentum-Based Electromagnetic Vortex Imaging," in IEEE Antennas and Wireless Propagation Letters, vol. 14, pp. 711-714, 2015

[6] T. Yang et al., "High-Resolution Vortex Electromagnetic Wave Radar Sparse Imaging Using Efficient 2D-SLIM," in IEEE Transactions on Computational Imaging, vol. 12, pp. 614-629, 2026,

[7] J. Wang, K. Liu, H. Liu, K. Cao, Y. Cheng and H. Wang, "3-D Object Imaging Method With Electromagnetic Vortex," in IEEE Transactions on Geoscience and Remote Sensing, vol. 60, pp. 1-12, 2022, Art no. 2000512

[8] T. Yang, H. Shi, J. Guo, X. Wang, Y. Liu and H. Cheng, "A Fast and High-Resolution Imaging Method for Electromagnetic Vortex Radar Using Uniform Concentric Circular Arrays," in IEEE Transactions on Microwave Theory and Techniques, vol. 73, no. 5, pp. 3004-3015, May 2025

[9] T. Yang, H. Shi, J. Guo and D. Liu, "3D Sparse ISAR Imaging With Multiple Plane Spiral OAM Electromagnetic Waves," in IEEE Sensors Journal, vol. 22, no. 15, pp. 15082-15097, 1 Aug.1, 2022

[10] K. Liu, X. Li, Y. Gao, Y. Cheng, H. Wang and Y. Qin, "High-Resolution Electromagnetic Vortex Imaging Based on Sparse Bayesian Learning," in IEEE Sensors Journal, vol. 17, no. 21, pp. 6918-6927, 1 Nov.1, 2017

[11] H. Qu, D. Cheng, C. Chen and W. Chen, "Sparsity-driven high-resolution fast electromagnetic vortex imaging based on two-dimensional NCALM," 2020 IEEE 6th International Conference on Computer and Communications (ICCC), Chengdu, China, 2020, pp. 1880-1885

[12] S. Wang, Y. Luo, Y. Chen, Y. Qu and J. Yan, "3-D Imaging With Vortex Electromagnetic Wave Radar Based on Nested Array Structure—Part I: Sparse Imaging Algorithm," in IEEE Sensors Journal, vol. 25, no. 23, pp. 42988-43002, 1 Dec.1, 2025

[13] H. Qu, C. Chen, J. Liu and W. Chen, "Enhanced Vortex Wavefront Modulated Radar Forward-Looking Variational Bayesian Hierarchical Structural Sparse Imaging by Leveraging the Continuity of Target Scene," in IEEE Transactions on Aerospace and Electronic Systems, vol. 61, no. 3, pp. 5962-5979, June 2025

[14] T. Jiang, J. Hu, S. Luo, Y. Wang and W. Wu, "A Fast and Super-Resolution Method of Vortex-Based Imaging," in IEEE Antennas and Wireless Propagation Letters, vol. 22, no. 9, pp. 2225-2229, Sept. 2023

[15] H. Qu, S. Li, C. Chen, J. Liu and W. Chen, "High-Resolution Orbital Angular Momentum Imaging With the Removal of Bessel Function Modulation Effect," in IEEE Transactions on Microwave Theory and Techniques, vol. 72, no. 4, pp. 2577-2590, April 2024

[16] Y. Zhu, Y. Zhou, Y. Chen, L. Bu and H. Zhao, "A Mode Optimization Method for Vortex Electromagnetic Wave Radar Imaging," in IEEE Geoscience and Remote Sensing Letters, vol. 19, pp. 1-5, 2022, Art no. 4024405